materials. The honeycomb diameter is only a few millimeters, the height of the material is several centimeters. The spacing between the layers interrupt the conduction of heat from the hot outer surface to the inner layer, which is responsible for the heat exchange with the cell. In systems with radii of $R_1 = 40$ cm and $R_2 = 80$ cm, $X$ values of 0.01 can be achieved. Such a skin structure is foreseen for the Twin-Solar-Probes, being designed for the European Space Research Organization (ESRO).[4]

The electrical output of the chopped system is reduced in the same proportion as the heat. For an optimized system with $x = 0.02$ and $R_1 = 40$ cm, the light passage is 5 cm and the constant power output of a 1 m-long stripe is approximately 7 w. Using storage batteries, this would be enough for deep space communications.

The weight balance is essential determined by the mass of the honeycomb skin. The 10 cm-thick honeycomb skin of the Twin-Solar-Probes has a mass of approximately 18 kg. The specific weight would be 0.4 w/kg. In spite of the low specific weight, the chopped system was found to be preferred to other systems. The main reasons were 1) The possibility of using normal solar cell techniques as close as 0.1. a.u. 2) Chopping doesn't require additional mechanisms and control elements. 3) The lifetime of the shielded cells are longer than in open systems, because the interaction time with particles is reduced. Further protection against ultraviolet, ion and meteoroid bombardments can be afforded by covering the rear side of the perforated skin with a transparent layer of a suitable protection material. 4) The reliability is much higher than in louver systems. Special high temperature requirements for the actuators and control mechanisms result in heavy systems. 5) As seen in the "Helios" research,[5] the use of solar cells, diluted with Second-Surface-Mirrors, are limited to distances of about 0.3 a.u.

## References

[1] Broder, J. D., Kautz, H. E., Mandelkorn, J., Schwartz, L., and Ulman, R. P., "Solar-Cell Performance at High Temperatures," TN D-2529, Dec. 1964, NASA.

[2] Preuss, L. "Testergebnisse an einem Solarzellenpanel für den Einsatz bei hohen Bestrahlungsstärken," *Raumfahrtforschung*, Vol. 14, Heft 5/1970, pp. 183–188.

[3] Suppa, E., Heinicke, J., Köhler, F., and Müller, E., "Neue technologische Verfahren für Solarzellenanlagen," *Raumfahrtforschung*, Vol. 13, Heft 5/1969, pp. 205–212.

[4] Eder, H., "Thermomechanical Performance of the Twin Solar-Probes System," Contract 1147/70/EL Contraves AG, Zurich, Switzerland, May 1971, European Space Research Organisation (ESRO), Paris.

[5] Koelle, E., "Entwurfskriterien und Alternativen für Sonnensonden mit 0.3 bis 0.1 A.E. Periheldistanz," *Raumfahrtforschung*, Vol. 13, Heft 3/1969, pp. 121–131.

MARCH 1973 J. SPACECRAFT VOL. 10, NO. 3

# Attitude Control of a Spinning Skylab

S. M. SELTZER*
*NASA Marshall Space Flight Center, Ala.*
AND
GERHARD SCHWEITZER†
*Technische Universitaet, Muenchen, Germany*
AND
BERNARD ASNER JR.‡
*Bogazici Universitesi, Istanbul, Turkey*

**Active attitude control of a spinning Skylab is analyzed to determine a simple control law that will provide a satisfactory response, considering the dynamics of attached flexible appendages. A simplified model of the complex Skylab vehicle is selected to make it analytically tractable. The vehicle is modeled as a single rigid-core body with two attached flexible massless booms having masses on their tips. The equations of motion describing the attitude dynamics of the model are presented as a linear matrix-differential equation. The states of the vehicle are small perturbations about its steady-state spin. An analysis is performed to determine the domain of stability. Next, attitude dynamics are analyzed; both frequency domain (parameter plane) and time domain (an optimal linear quadratic loss program) techniques are compared. An analysis of the nonlinear effect of control torque saturation of Skylab's control moment gyroscopes is discussed. The results of the analysis compare favorably with a large-scale digital simulation of the Skylab.**

## Introduction

IN 1970, NASA initiated a set of studies of several Skylab configurations, including a spinning vehicle configuration. The spin would provide an artificial-gravity environment to assess and compare the physiological benefits and problems of prolonged zero-gravity and artificial-gravity environments. The results of this study should be appropriate not only for the Skylab configuration but also for analysis of future spacecraft, particularly those that are composed of several connected bodies with attached flexible appendages. However, the presently approved Skylab program does not include a spinning vehicle.

In spinning the Skylab, the vehicle must spin about the principal axis of intermediate moment of inertia (in the original nonspinning Skylab configuration) to keep the solar panels pointed nominally toward the sun. In an effort to achieve passive stability, masses were deployed either on cables or extended booms so that the principal axis of maximum moment of inertia could point in the same direction as the solar panels. An analysis has indicated that passive stability can be achieved.[1] Geometric asymmetries of the original Skylab require that the extendable booms be attached out of the original plane of rota-

Presented as Paper 72-889 at the AIAA Guidance and Control Conference, Stanford, Calif., August 14–16, 1972; submitted August 16, 1972; revision received October 31, 1972. The coauthors gratefully acknowledge the support of the National Research Council, which made it possible for G. Schweitzer to work on this research as a NASA Postdoctoral Resident Research Associate during 1970–71.

Index categories: Manned Space Station Systems; Spacecraft Attitude Dynamics and Control.

* Senior Research Scientist, Astrionics Laboratory. Associate Fellow AIAA.

† Akademischer Oberrat, Institut B fuer Mechanik.

‡ Assistant Professor, Mathematics Department.

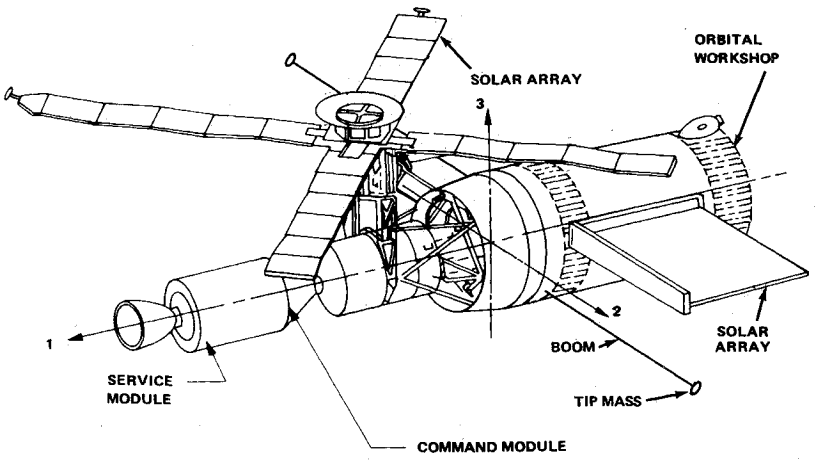


Fig. 1 Skylab.

tion to make the desired rotation axis an axis of principal inertia. Although the out-of-plane distance of the booms is small compared with their lengths, its effect is considered.

A study team at the Marshall Space Flight Center has completed a preliminary analysis of this problem.[2] The analysis gives a more detailed study of the control problem to include consideration of certain nonlinear characteristics and several approaches to formulating a simple attitude control law.

The primary objective of the study reported here is to analyze active attitude control of a spinning Skylab. To achieve financial economy, the study is constrained to the use of existing Skylab onboard equipment, including control moment gyroscopes (CMG's).[3] It is desired to determine a control law that will provide satisfactory control in terms of damping out initial errors in vehicle attitude and attitude rate, considering the dynamics of the attached flexible appendages. The resulting control law should be simple both to implement and to analyze. (A secondary objective is to provide a physical explanation for the motion predicted by the analysis.) Finally, areas of improvement should be determined, both by specifying performance criteria more precisely and by optimizing control parameters used in the postulated control laws.

The method of approach is first to define a realistic model and then to derive or state the applicable equations of motion. Next, a control law is postulated that considers the saturation characteristics of the CMG's; i.e., a limited amount of available momentum. A stability analysis is then performed, considering linear operation, and the transient characteristics of vehicle motion are determined for various choices of control parameters. Also considered is the effect of a limited amount of control torque.

## Model Definition and Equations of Motion

The complex Skylab vehicle (Fig. 1) is simplified to make it analytically tractable. The vehicle is modeled as a single rigid-core body with two attached flexible massless booms having masses on their tips (Fig. 2). The small angle $\phi$ between the solar vector and the 3-axis is resolved into angular rotations $\phi_1$ and $\phi_2$ about the 1- and 2-axes, respectively. The angular velocity of the vehicle is written in body-fixed coordinates 1, 2, 3 in terms of small perturbations $w_i$ ($i = 1, 2, 3$) about the steady-state velocity $\Omega$. The integral of the variations in angular velocity about the 3-axis is denoted by $\phi_3$. Variables $u_i^k$ ($i = 1, 2, 3$; $k = \mathrm{I}, \mathrm{II}$) represent small displacements of each of the two tip masses ($m$) from the steady-state. In the steady-state, the principal axes of inertia coincide with the 1, 2, 3 axes and the principal moments of inertia are denoted by $I_1, I_2, I_3$, respectively, with $I_1 < I_2 < I_3$. Boom stiffness in the 1, 2, and 3 directions is characterized by the stiffness coefficients $k_1$, $k_2$, and $k_3$, respectively, of the nonrotating boom. In this case, it is assumed that the booms are attached on the core body sufficiently close to the spin axis. For a more detailed analysis, the actual nonzero distance between the spin axis and the roots of the booms influences the stiffness parameters and the effective inertia of the tip masses and should be taken into account.[4] Structural damping of the boom is proportional to elastic deformation velocities and is denoted in the 1, 2, and 3 directions as $d_1$, $d_2$, and $d_3$, respectively. The steady-state coordinates of the tip masses are $\Gamma_i^I = -\Gamma_i^{II}$ and are shown in Fig. 2. The translational and rotational equations of motion associated with the simplified model may be derived by the application of Newton's and Euler's relationships, respectively, and are described extensively by Likins for the general case of a rotating vehicle containing spinning rotors and having arbitrary flexible appendages attached.[5] The general equations of motion may be simplified and presented as a matrix equation describing the attitude of the vehicle

$$\mathbf{M}\mathbf{z}'' + \mathbf{D}\mathbf{z}' + \mathbf{K}\mathbf{z} = -\mathbf{v} \tag{1}$$

where

$$\mathbf{z} = [\phi_1, \phi_2, \mu_3, \phi_3, \mu_1, \mu_2]^T \tag{2}$$

$$\mathbf{v} = [v_1, v_2, 0, v_3, 0, 0]^T = [T_1/I_1\Omega^2, T_2/I_1\Omega^2, 0, T_3/I_1\Omega^2, 0, 0]^T \tag{3}$$

$$\mathbf{M} = \begin{bmatrix} 1 & 0 & -\gamma & 0 & 0 & \gamma\Gamma_3/\Gamma_2 \\ 0 & 1 + K_1/1 - K_2 & 0 & 0 & -\gamma\Gamma_3/\Gamma_2 & 0 \\ -\gamma & 0 & \gamma & 0 & 0 & 0 \\ 0 & 0 & 0 & I_3/I_1 & \gamma & 0 \\ 0 & -\gamma\Gamma_3/\Gamma_2 & 0 & \gamma & \gamma & 0 \\ \gamma\Gamma_3/\Gamma_2 & 0 & 0 & 0 & 0 & \gamma \end{bmatrix} \tag{4}$$

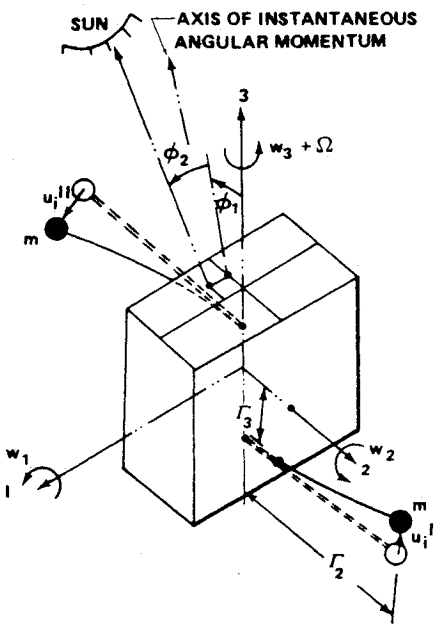


Fig. 2 Variables for attitude control.

$$\mathbf{D} = \begin{bmatrix} 0 & -(1+K_1) & 0 & 0 & 2\gamma\Gamma_3/\Gamma_2 & 0 \\ 1+K_1 & 0 & 0 & 0 & 0 & 2\gamma\Gamma_3/\Gamma_2 \\ 0 & 0 & \gamma\Delta_3 & 0 & 0 & 0 \\ 0 & 0 & 0 & 0 & 0 & -2\gamma \\ -2\gamma\Gamma_3/\Gamma_2 & 0 & 0 & 0 & \gamma\Delta_1 & -2\gamma \\ 0 & -2\gamma\Gamma_3/\Gamma_2 & 0 & 2\gamma & 2\gamma & \gamma\Delta_2 \end{bmatrix} \quad (5)$$

$$\mathbf{K} = \begin{bmatrix} -K_1 & 0 & -\gamma & 0 & 0 & -\gamma\Gamma_3/\Gamma_2 \\ 0 & K_2\left(\frac{1+K_1}{1-K_2}\right) & 0 & 0 & \gamma\Gamma_3/\Gamma_2 & 0 \\ -\gamma & 0 & \gamma(\sigma_3^2+1) & 0 & 0 & 0 \\ 0 & 0 & 0 & 0 & 0 & 0 \\ 0 & \gamma\Gamma_3/\Gamma_2 & 0 & 0 & \gamma\sigma_1^2 & 0 \\ -\gamma\Gamma_3/\Gamma_2 & 0 & 0 & 0 & 0 & \gamma(\sigma_2^2-1) \end{bmatrix} \quad (6)$$

The symbols are defined as

$$K_1 = /I_2 - I_3)/I_1, \quad K_2 = (I_3 - I_1)/I_2, \quad \gamma = 2m\Gamma_2^2/I_1 \quad (7)$$
$$\Delta_i = d_i/m\Omega, \quad \sigma_i^2 = k_i/m\Omega^2, \quad (i = 1, 2, 3)$$

and $'$ refers to differentiation with respect to $\tau = \Omega t$. Applied torque about the $i$-axis is represented by $T_i$ $(i = 1, 2, 3)$, and $\mu_i$ represents the elastic deformation characterizing the skew-symmetric mode

$$\mu_1 = (u_i^I - u_i^{II})/2\Gamma_2 \quad (8)$$

Because the quantity $\Gamma_3$ is small compared with other Skylab dimensions used in the analysis, it will be assumed to be zero during the initial analysis. The effect of nonzero $\Gamma_3$ will be considered later. If $\Gamma_3 = 0$, the six equations represented in matrix Eq. (1) become uncoupled into two sets of three equations each: the wobble motion, described by $\phi_1, \phi_2, \mu_3$, and the in-plane motion, described by $\phi_3, \mu_1, \mu_2$. A new matrix equation for the wobble motion is written as

$$My'' + Dy' + Ky = -v \quad (9)$$

where

$$y = [\phi_1, \phi_2, \mu_3]^T \quad (10)$$

$$v = [T_1/I^1\Omega^2, T_2/I_1\Omega^2, 0]^T \quad (11)$$

and the new $M$, $D$, $K$ matrices are obtained from Eqs. (4–6) by setting $\Gamma_3 = 0$ and taking the upper left $3 \times 3$ matrices.

## Control Law

The mission of a spinning Skylab requires that the 3-axis be pointed at the sun. To maintain the 3-axis inertially fixed (moving it slightly at discrete intervals to realign it toward the sun), attitude control torques must be applied to the vehicle to compensate for the effect of disturbance torques. These control torques must in some manner depend on error signals that are proportional both to the angle between the 3-axis and the solar vector and to its time derivative. Existing Skylab hardware includes sun sensors and rate gyros capable of generating this information. The sun sensors measure the angular rotations $\phi_1$, $\phi_2$, and rate gyros measure the angular velocities $w_1$, $w_2$. The control torques $T_1$, $T_2$ are provided by the CMG's and may be augmented if necessary by a mass expulsion system; it is assumed that $T_3 = 0$. A linear control postulate is formulated as

$$\begin{bmatrix} T_1 \\ T_2 \end{bmatrix} = \begin{bmatrix} \alpha_{11} & \alpha_{12} \\ \alpha_{21} & \alpha_{22} \end{bmatrix} \begin{bmatrix} \phi_1 \\ \phi_2 \end{bmatrix} + \begin{bmatrix} \beta_{11} & \beta_{12} \\ \beta_{21} & \beta_{22} \end{bmatrix} \begin{bmatrix} w_1 \\ w_2 \end{bmatrix} \quad (12)$$

where, from kinematic relations

$$\begin{bmatrix} w_1 \\ w_2 \end{bmatrix} = \begin{bmatrix} -1 & 0 \\ 0 & -1 \end{bmatrix} \begin{bmatrix} \phi_1 \\ \phi_2 \end{bmatrix} + \begin{bmatrix} 0 & \Omega \\ -\Omega & 0 \end{bmatrix} \begin{bmatrix} \phi_1 \\ \phi_2 \end{bmatrix} \quad (13)$$

and $\cdot$ refers to differentiation with respect to time. To simplify the analysis, only a few control parameters are used. A controllability analysis shows that the wobble motion can be controlled by a control torque applied about a single axis, i.e., the 1-axis. This requires retention of the control gains $\alpha_{11}$, $\alpha_{12}$, $\beta_{11}$, and $\beta_{12}$. Gyrodynamics of a rigid body show that a nutation angle is effectively influenced by applying a torque orthogonal to both the spin axis and the axis of the inclination angle. This physical explanation suggests the retention of gain $\alpha_{12}$, thus influencing the inclination $\phi_2$ by a torque about the 1-axis. Feedback of the angular velocity to damp the nutation requires a control gain $\beta_{11}$. Only $\alpha_{12}$ and $\beta_{11}$ are used in the following development and are redefined for subsequent convenience as

$$\varepsilon = \alpha_{12}/I_1\Omega^2, \qquad \delta = \beta_{11}/I_1\Omega \quad (14)$$

An inclusion of other control variables into the linear control law is considered in the section on Choice of Parameters and Transient Response ($\Gamma_3 = 0$). If limited control torque is available, a nonlinear modification of the control law must be considered [Effect of Control Torque Saturation ($\Gamma_3 = 0$) section].

## Linear Stability Analysis for Model with In-Plane Booms ($\Gamma_3 = 0$)

If it is assumed that the control is linear and about the 1-axis so that the only control gains are $\delta$, $\varepsilon$ [Eq. (14)], then the characteristic polynomial associated with Eqs. (9) and (10) becomes

$$p(\lambda) = \sum_{j=0}^{6} (a_j\delta + b_j\varepsilon + c_j)\lambda^j = 0 \quad (15)$$

Here,

$$\lambda \equiv s/\Omega = \eta + iv \quad (16)$$

where $\lambda$ is the normalized Laplace operator; i.e., $\mathscr{L}[\phi] = s\Phi(s)$ and $\mathscr{L}[\phi'] = \lambda\Phi(\lambda)$. Coefficients $a_j$, $b_j$, and $c_j$ are defined in Table 1. Stable regions in terms of control parameters $\delta$ and $\varepsilon$ may be determined by the $D$-decomposition method.[6] Generally, two stability boundaries can be found by setting the coefficients $\lambda^0$ and $\lambda^6$, respectively, equal to zero. In this example, the resulting boundaries are independent of $\delta$ and $\varepsilon$ and will not appear on the $\delta$–$\varepsilon$ control parameter plane. However, the boundaries associated with complex conjugate roots do appear and are found by setting $\eta = 0$ in Eq. (15) and writing the real and imaginary parts of the equation as two separate equations

$$\begin{aligned} \text{Re } p(iv) &= (1-v^2)\delta + (1-K_2)\varepsilon \\ &= -(1-v^2)[-\gamma(1-v^2)(K_2-v^2) + \\ &\qquad (v^2-\sigma_3^2-1)(v^2+K_1K_2)]/\Delta_3 v^2 \end{aligned} \quad (17)$$

and

$$\begin{aligned} \text{Im } p(iv) &= (1-v^2)\delta + (1-K_2)\varepsilon \\ &= \Delta_3(K_1K_2+v^2)(1-v^2)/(v^2-\sigma_3^2-1) \end{aligned} \quad (18)$$

Since the left-hand sides of Eqs. (17) and (18) are identical, the right-hand sides may be set equal to each other; this yields the product of a cubic equation and a linear equation in $v^2$

$$\begin{aligned} (1-v^2)\{&(1-\gamma)v^6 + [\Delta_3^2 + K_1K_2 + \gamma(K_2+1) - \\ &(\sigma_3^2+1)(2-\gamma)]v^4 + \\ &\{\Delta_3^2K\ K_2 - \gamma[K_2 + (\sigma_3^2+1)(K_2+1)] + \\ &(\sigma_3^2+1)(\sigma_3^2+1-2K_1K_2)\}v^2 + (\sigma_3^2+1)K_2 \\ &[\gamma + K_1(\sigma_3^2+1)]\} = 0 \end{aligned} \quad (19)$$

**Table 1 Characteristic equation coefficients**

| $j$ | $a_j$ | $b_j$ | $c_j$ |
|---|---|---|---|
| 0 | 0 | 0 | $-K_2[\gamma + K_1(\sigma_3^2+1)]$ |
| 1 | $-(\sigma_3^2+1)$ | $-(\sigma_3^2+1)(1-K_2)$ | $-\Delta_3K_1K_2$ |
| 2 | $-\Delta_3$ | $-\Delta_3(1-K_2)$ | $\sigma_3^2 + 1 - K_1K_2(2+\sigma_3^2) - \gamma(1+2K_2)$ |
| 3 | $-(2+\sigma_3^2)$ | $-(1-K_2)$ | $\Delta_3(1-K_1K_2)$ |
| 4 | $-\Delta_3$ | 0 | $2 - K_1K_2 + \sigma_3^2 - \gamma(K_2+2)$ |
| 5 | $-1$ | 0 | $\Delta_3$ |
| 6 | 0 | 0 | $1-\gamma$ |

**Table 2 Physical characteristics of Skylab**

| |
|---|
| $I_1 = 1.25 \times 10^6$ kg m$^2$ |
| $I_2 = 6.90 \times 10^6$ kg m$^2$ |
| $I_3 = 7.10 \times 10^6$ kg m$^2$ |
| $\Gamma_1 = 0$ |
| $\Gamma_2 = 23.3$ m |
| $\Gamma_3 = -1.53$ m |
| $m = 227$ kg |
| $k_1 = k_3 = 146$ N/m |
| $k_2 = 7.4 \times 10^4$ N/m |
| $d_1 = d_3 = 0.04\,(k_3\ \text{m})^{1/2}$ |
| $d_3 = 0.04\,(k_2\ \text{m})^{1/2}$ |
| $\Omega = 0.6\ \text{s}^{-1}$ |

Substituting the solution, $\nu^2 = 1$, into either Eqs. (17) or (18) yields a stability boundary

$$\varepsilon = 0 \tag{20}$$

The remaining three values of $\nu^2(\nu_1^2, \nu_2^2, \nu_3^2)$ are found by solving the cubic portion of Eq. (19) and substituting them one at a time into either Eqs. (17) or (18), resulting in three straight lines on the $\delta$–$\varepsilon$ plane. At this point, numerical values typical of the Skylab are introduced in Table 2.[3]

If Table 2 values are substituted into Eq. (19) and the resulting values for $\nu_1$, $\nu_2$, $\nu_3$ (0.2854, 1.7500, and 1.6806, respectively) are substituted into Eqs. (17) and (18), the resulting three straight lines and Eq. (20) are plotted on the $\delta$–$\varepsilon$ parameter plane (Fig. 3). The encircled numbers represent the number of stable roots of Eq. (15) in each of the regions on the $\delta$–$\varepsilon$ plane. The boundary associated with $\nu_1^2$ is considered as a rigid-body stability boundary influenced by the boom elasticity; the $\nu_2^2$ boundary is primarily influenced by the elastic boom motion, and the $\nu_3^2$ boundary results from a combination of rigid-body and elastic-boom motion. The effect of boom flexibility on stability may be seen by comparing the true rigid-body stability boundary with the $\nu_1^2$ boundary. The rigid-body stability boundaries are found by setting $\gamma$ and $1/\sigma_3^2$ both equal to zero in Eq. (19) and solving for $\nu^2$. This yields two values of $\nu^2$: $-K_1K_2$ and 1. The rigid-body stability boundaries are found by substituting these values into either Eqs. (17) or (18); this yields

$$\varepsilon = -[(1 + K_1K_2)/(1 - K_2)]\delta \tag{21}$$

and Eq. (20). The boundary of Eq. (21) may be compared with the $\nu_1^2$ boundary of the flexible body to determine the effect of flexibility on the stable region (Fig. 4).

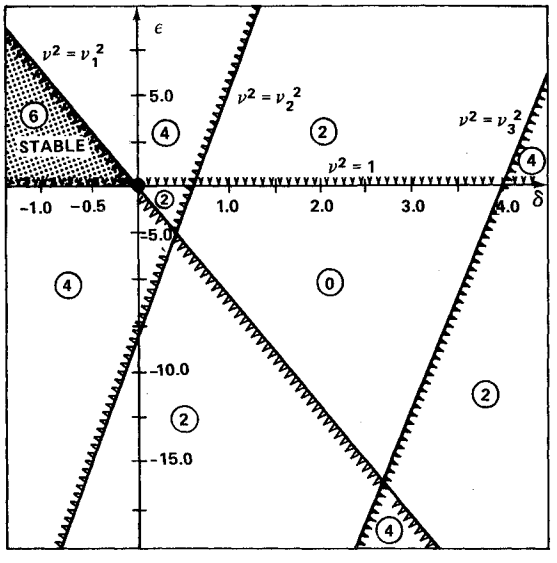


NOTE: ENCIRCLED NUMBERS INDICATE NUMBER OF STABLE ROOTS IN REGION

**Fig. 3 Stability boundaries.**

## Damping Characteristics for Model with In-Plane Booms ($\Gamma_3 = 0$)

The parameter plane technique[6] is applied to Eq. (15) and Table 1 to plot contours of constant damping ratio $\zeta$ as functions of the normalized natural frequency $\nu_n$, where

$$\nu_n = (\nu^2 + \eta^2)^{1/2} \qquad \text{and} \qquad \zeta = \eta/(\nu^2 + \eta^2)^{1/2} \tag{22}$$

These contours are associated with the complex conjugate roots of Eq. (15) and are plotted on the $\delta$–$\varepsilon$ control parameter plane from Eqs. (23)

$$\delta = (B_1C^2 - B_2C_1)/J \qquad \varepsilon = (A_2C_1 - A_1C_2)/J \tag{23}$$

where the Jacobian $J$ is

$$J = A_1B_2 - A_2B_1 \tag{24}$$

and

$$A_1 = \sum_{j=0}^{6} a_jX_j, \qquad B_1 = \sum_{j=0}^{6} b_jX_j, \qquad C_1 = \sum_{j=0}^{6} c_jX_j$$

$$A_2 = \sum_{j=0}^{6} a_jY_j, \qquad B_2 = \sum_{j=0}^{6} b_jY_j, \qquad C_2 = \sum_{j=0}^{6} c_jY_j \tag{25}$$

$$\lambda^j = X_j + iY \tag{26}$$

Values for $X_j$ and $Y_j$ are found from the recursive relationships

$$X_{j+1} = -2\zeta\nu_nX_j - \nu_n^2X_{j-1}$$
$$Y_{j+1} = -2\zeta\nu_nY_j - \nu_n^2Y_{j-1} \tag{27}$$

and $X_0$, $Y_0$, $X_1$, and $Y_1$ are found from Eq. (26). The technique involves choosing a numerical value for $\zeta$, solving Eqs. (23) for $\delta$ and $\varepsilon$ as functions of $\nu_n$, and plotting the resulting $\delta$ contours on the $\delta$–$\varepsilon$ plane. The process is repeated for various choices of $\zeta$. Real root contours associated with real roots of Eq. (15) are calculated from the equation

$$\varepsilon = -(A_3/B_3)\delta - (C_3/B_3) \tag{28}$$

where

$$A_3 = \sum_{j=0}^{6} a_j\eta^j, \qquad B_3 = \sum_{j=0}^{6} b_j\eta^j, \qquad C_3 = \sum_{j=0}^{6} c_j\eta^j \tag{29}$$

From the real root and $\zeta$ contours on the $\delta$–$\varepsilon$ plane, one can determine the expected transient characteristics of the motion of the vehicle for various values of control parameters $\delta$ and $\varepsilon$. The expected characteristics may be compared with the actual characteristics determined next. Typical $\zeta$ contours in the stable region of the $\delta$–$\varepsilon$ plane for Skylab characteristics (Table 2) are shown in Fig. 5.

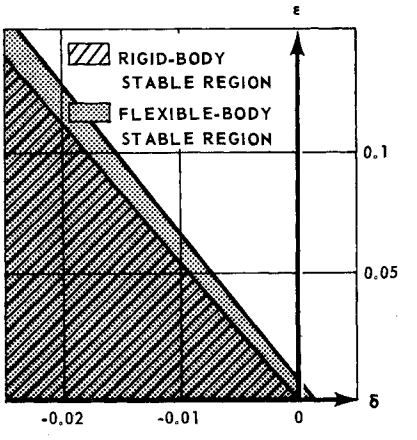


**Fig. 4 Stability region for wobble motion in the control parameter plane.**

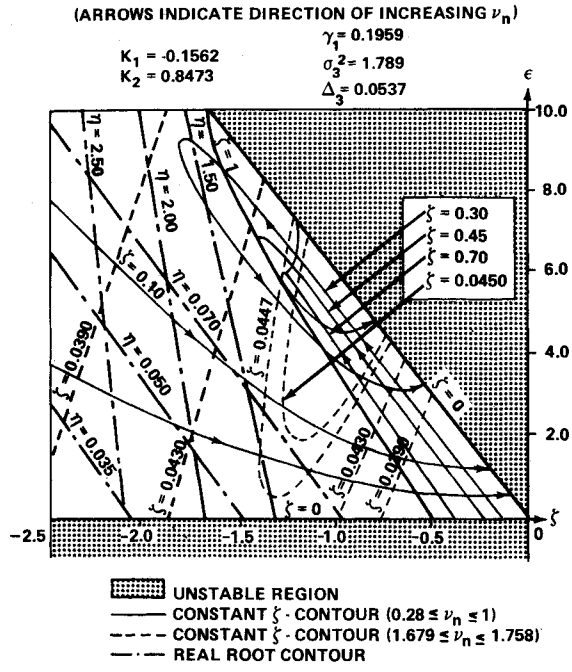


Fig. 5 Damping characteristics.

## Choice of Parameters and Transient Response ($\Gamma_3 = 0$)

Two approaches are used to determine values of control gains $\alpha_{ij}$, $\beta_{ij}$ for the model with the in-plane booms. The first is to consider desirable damping characteristics using the parameter plane map. The second approach is to use a linear quadratic loss (LQL) program and to minimize a performance index by optimal choice of the control gains.

If the control torque is to be applied about only one axis and control gains $\delta$ and $\varepsilon$ ($\alpha_{12}$, $\beta_{11}$) are considered, the parameter plane (Fig. 5) may be used to choose numerical values for these gains. An example of this approach is to assume that only the regions of the parameter plane having three stable pairs of complex conjugate roots will be considered, i.e., the region bounded by the $\zeta = 0$ contour and the aperiodic $\zeta = 1$ contour. This region is shown in more detail in Fig. 6. For clarity the $\zeta$ contours associated with the weakly damped $\mu_3$ boom motion (Fig. 5) have been omitted from Fig. 6 since the corresponding pair of complex conjugate roots varies only slightly for the various choices of $\delta$ and $\varepsilon$ that will be considered. If it is desired to set $\zeta = 0.707$ for both pairs of complex conjugate roots (Fig. 6), values of $\delta = -1.27$ and $\varepsilon = 5.9$ are selected, resulting in $\nu_n = 0.560$ for both pairs of roots. The third pair of complex conjugate roots has values of $\zeta = 0.045$ and $\nu_n \approx 1.7$. Corresponding time responses are shown in Fig. 7. As predicted, $\phi_1$ and $\phi_2$ responses are well-damped oscillations with periods nearly the same as the rigid-body period (Fig. 6). The $\mu_3$ motion is lightly damped and oscillatory. Alternatively, the control system designer might decide to permit lightly damped oscillatory behavior of the rigid-body motions, but bounded by strong exponential damping. Figure 5 indicates such behavior in the vicinity $\delta = -1.00$, $\varepsilon = 2.0$. At that point, two pairs of lightly damped complex

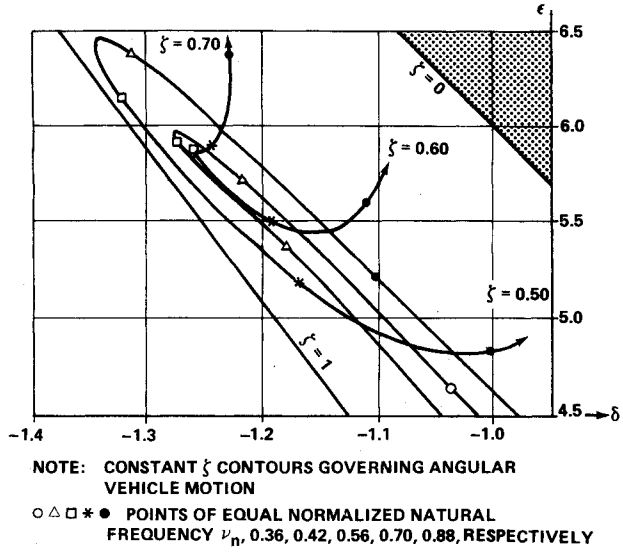


Fig. 6 Damping characteristics (selected region of Fig. 5).

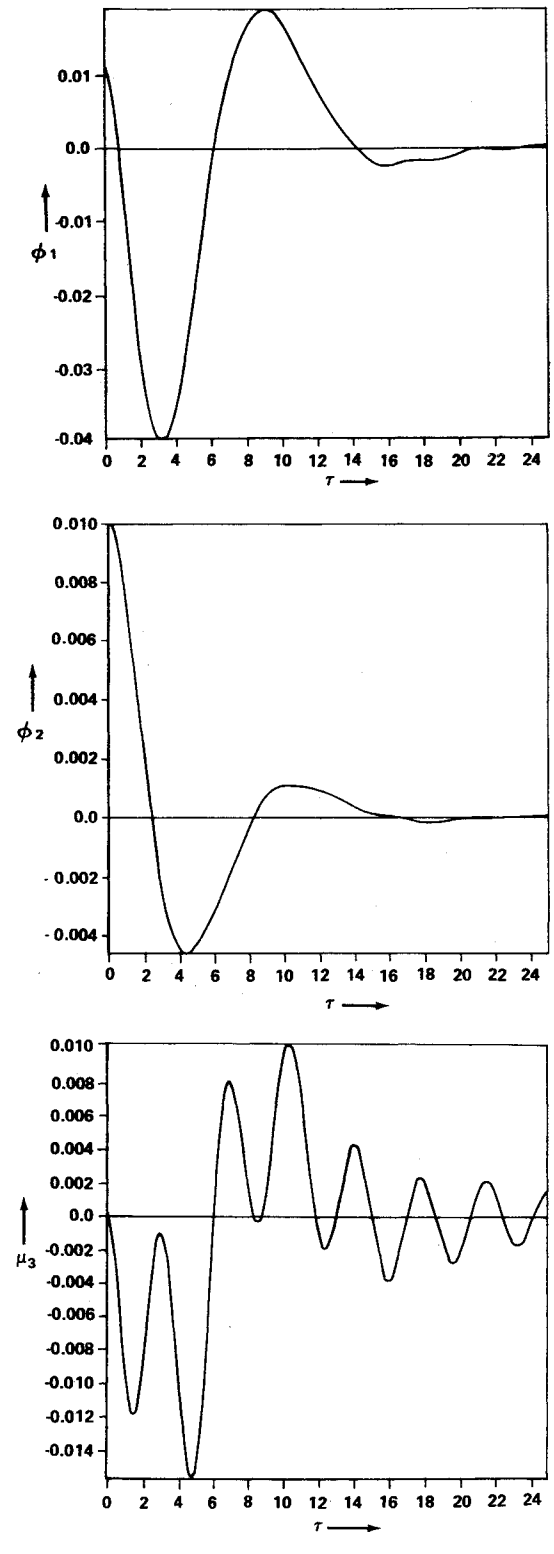


Fig. 7 Time response for control gains $\delta = -1.27$, $\varepsilon = 5.9$.

conjugate roots ($\zeta = 0.045$, $\nu_n = 1.72$; $\zeta = 0.10$, $\nu_n = 0.98$) and a pair of real roots ($\eta = -0.507$ and $-0.0741$) exist. The damping of the system motion is dominated by the real root closest to the origin. Time responses of $\phi_1$, $\phi_2$, and $\mu_3$ (Fig. 8) confirm the expected behavior.

The LQL program[7] may be used to determine optimal values for the control gains $\alpha_{ij}$, $\beta_{ij}$ by minimizing the performance index

$$\text{PI} = \int_0^{\tau_f} (x^T Q x + v^T R v)\, d\tau \tag{30}$$

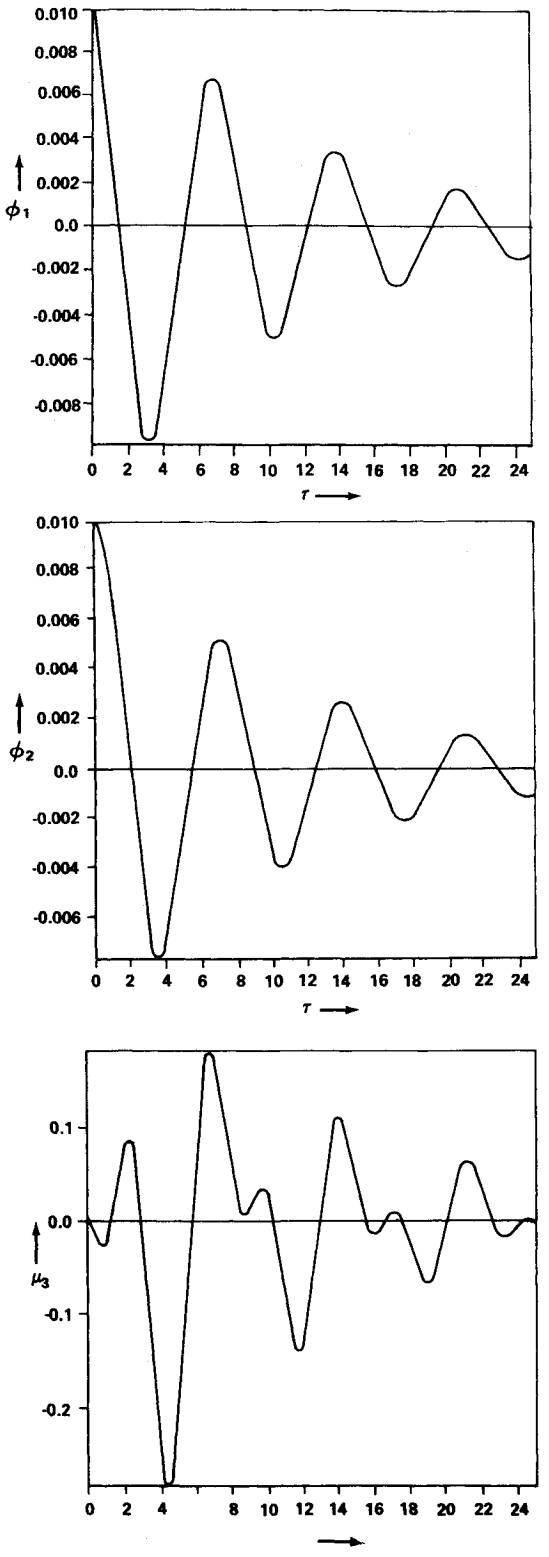


**Fig. 8 Time response for control gains $\delta = -1.00$, $\varepsilon = 2.0$.**

where the $x$ and $v$ represent the state ($n \times 1$) and control ($m \times 1$) vectors in the state-space equation

$$x' = Fx + Gv \tag{31}$$

where $x = [y^T \mid y'^T]^T$ and $v = [v_1, v_2, 0]^T$; $y$ and $v$ are defined in Eqs. (10) and (11). Using the notation of Eq. (9), the open-loop state distribution matrix $F$ and the control distribution matrix $G$ are defined as follows

$$F = \left[\begin{array}{c|c} 0 & E_3 \\ \hline -M^{-1}K & -M^{-1}D \end{array}\right] \tag{32}$$

and

$$G = [0 \mid -M^{-1}]^T \tag{33}$$

where $E_3$ represents a $3 \times 3$ unit matrix. The feedback control is defined as $v = Cx$, where the optimal gain matrix $C$ is determined by minimizing the performance index. Elements of the cost-state weighting matrix $Q$ and cost-control weighting matrix $R$ are chosen to emphasize various aspects of the performance index. If control is restricted to that about the 1-axis only, then the $v$ vector is the element $v_1$ and the $G$ matrix consists only of the first column. If $Q$ is chosen so that the $x_3$ and $x_6$ motions (representing elastic boom deformations) are not weighted and $x_4$ and $x_5$ motions (representing body attitude rates) are weighted more heavily than $x_1$ and $x_2$ motions (representing body attitudes), a rule of thumb suggests the selection of values for elements of the $Q$ and $R$ matrices.[8] Elements of the inverses of the two matrices consist of the maximum acceptable values of the diagonals $x(\tau)x^T(\tau)$ and $v(\tau)v^T(\tau)$, respectively; each is multiplied by a weighting factor which is the scalar resulting from the multiplication of $\tau_f$ by $n$ and $m$, respectively. The terminal time $\tau_f$ of Eq. (30) should be chosen so that at least one period of the lowest mode is contained within the interval of integration. In the Skylab example, the lowest period corresponds to the lowest dimensionless frequency ($\nu$) that is expected in the analysis: $\nu \approx 0.24$ (Fig. 6), yielding $\tau_f \approx 25$. Since $n = 6$ and $m = 1$, weighting factors for $Q^{-1}$ and $R^{-1}$ are 125 and 25, respectively. The attitude variables $\phi_1$ and $\phi_2$ are expected to remain bounded by $10^{-2}$ rad and $\phi_1'$ and $\phi_2'$ by $0.6 \times 10^{-2}$ rad. The bounds on variables $\mu_3$ and $\mu_3'$ are assumed to be unrestricted. The maximum acceptable value for the $x(\tau)$ is thus $[10^{-2}, 10^{-2}, 0, 0.6 \times 10^{-2}, 0.6 \times 10^{-2}, 0]^T$, yielding a $Q$ matrix of

$$Q = \text{diag}\,[66, 66, 0, 185, 185, 0] \tag{34}$$

The maximum control torque ($T_s$) available from the three CMG's is 500 Nm, yielding a maximum value for the control variable $v_{\max} = 0.111 \times 10^{-2}$. To insure that this limit is not reached in the linear analysis, it is increased by a factor of 30, yielding a one element matrix, $R = 36$. Applying the LQL program to minimize Eq. (30), one obtains the linear feedback coefficient matrix $C = [1.263, -0.777, -0.172, 2.768, -1.792, -0.095]$. Figure 9 shows the corresponding time responses.

A comparison of the three sets of results (Figs. 7, 8, and 9) shows that Fig. 7 provides the best damping characteristics for core-body rotational motion but yields significantly higher overshoots early in the response. The parameter plane responses of Fig. 8 compare favorably with the LQL response of Fig. 9 for core-body attitude. However, the control postulate of Eq. (12) ignores boom motion, whereas the LQL control assumes control of all states. Consequently, the boom motion of Figs. 7 and 8 is considerably larger than that of Fig. 9. The LQL control torque,

$$v_1 = \sum_{j=1}^{6} c\, x_j,$$

depends primarily on core-body attitude and attitude rate since the numerical values of $c_3 x_3$ and $c_6 x_6$ are relatively small. Hence, if $c_3$ and $c_6$ were eliminated, one would expect no significant effect on the required control torque or the core-body motion. However, the boom motion would become significant, such as in the parameter plane cases. The problem of including the boom motion states in the LQL control is that they must be

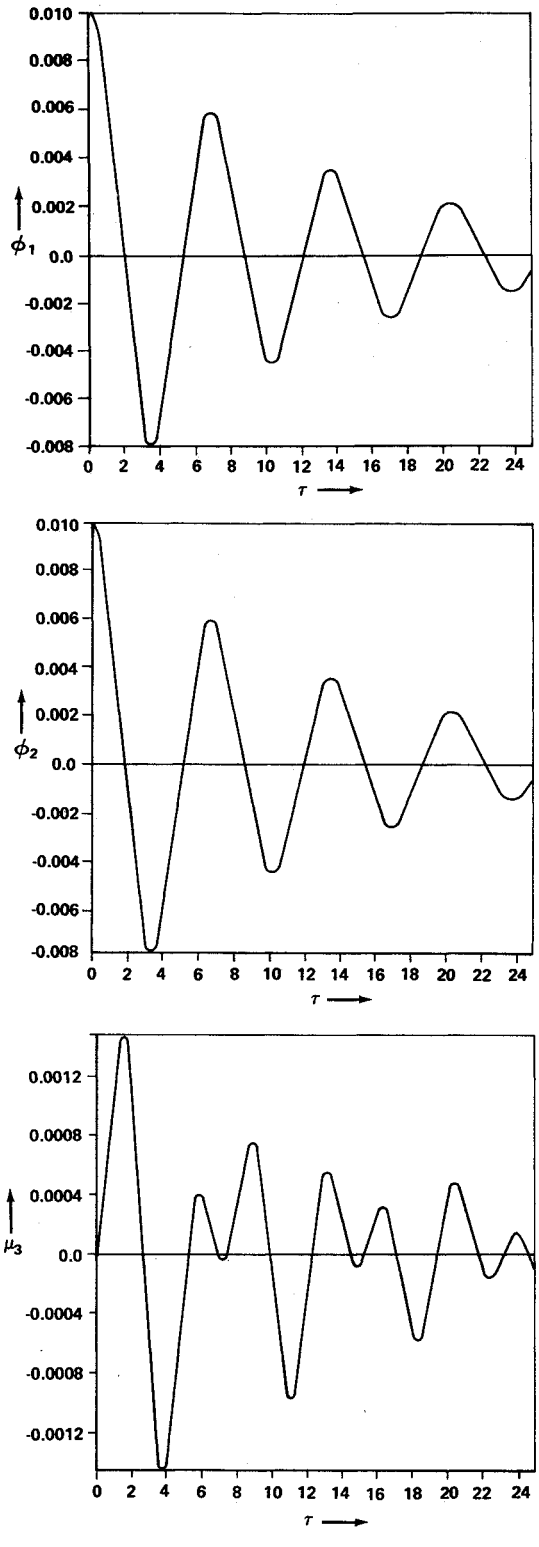


**Fig. 9 Time response for LQL control gains.**

measured or estimated with the attendant additional onboard complexity. If this complexity is warranted, the control postulate of Eq. (12) could similarly be modified by adding one or two terms to include $\mu_3$ and $\mu_3'$.

The main advantage of working with the parameter plane appears to be that it provides a quick design approach for relatively simple control systems. It yields physical insight into the stability and transient characteristics of the motion. However, for systems of higher order, its application becomes cumbersome. The main advantage of determining optimal control gains from a quadratic performance function is that the number of control inputs can easily be extended to higher-order cases, such as control about two axes. However, this technique requires knowledge of all states of the system. Further work on pole assignment techniques and criteria for choosing the weighting matrix $Q$ is indicated, such as the relation between the $Q$ matrix and selected eigenvalues.[9]

## Effect of Out-of-Plane Booms ($\Gamma_3 \neq 0$)

The effect of considering the flexible booms not lying in a plane perpendicular to the spin axis in steady-state is to couple the in-plane and out-of-plane motions. Instead of considering only a sixth-order characteristic equation governing wobble (out-of-plane) motion, now one must consider a twelfth-order equation associated with Eqs. (1) and (2). The variation ($\phi_3$) of the spin leads to two zero roots. If $D$-decomposition is applied to the remaining tenth-order characteristic equation, the stability diagram of Fig. 10 results. For the Skylab design problem ($\Gamma_3/\Gamma_2 \leqslant 0.07$), the primary stable region for $\Gamma_3 \neq 0$ is essentially unchanged from the region for uncoupled motion (Fig. 3). The four stability boundaries of Fig. 3 are easily recognized in Fig. 10. The change in character lies in the large lobes (shown by dashed lines) and the small additional stable region in the third quadrant. Although of academic interest, this region is of no consequence for the Skylab problem. It may be concluded that the simplified model with in-plane booms ($\Gamma_3 = 0$) will suffice for preliminary design of the spinning Skylab attitude control system.

## Effect of Control Torque Saturation ($\Gamma_3 = 0$)

For the case where control variables cause the desired torque to exceed the available torque, nonlinear operation is indicated. For the $\Gamma_3 = 0$ case and control about the 1-axis only, the

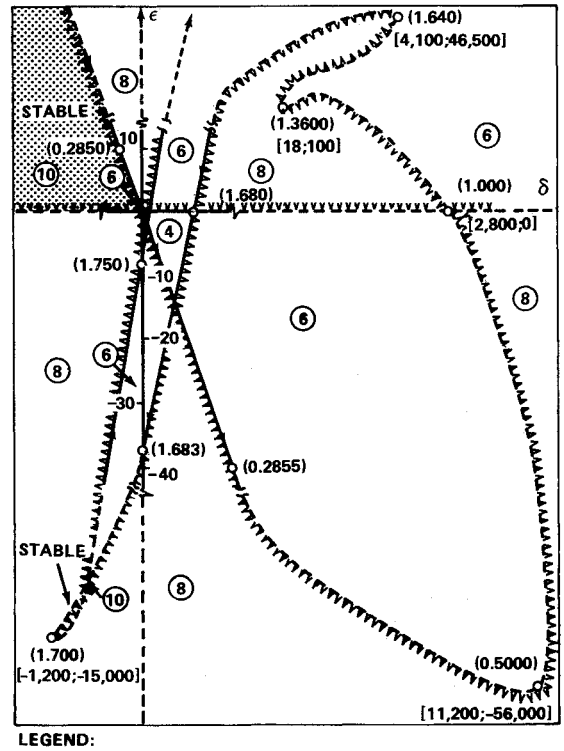


**LEGEND:**
- **NUMBERS IN BRACKETS REFER TO COORDINATES OF ADJACENT POINT.**
- **NUMBERS IN PARENTHESES REFER TO NORMALIZED FREQUENCY $\nu_n$ CORRESPONDING TO ADJACENT POINT.**
- **ENCIRCLED NUMBERS REFER TO NUMBER OF STABLE ROOTS IN REGION.**

**Fig. 10 Stability boundaries for $\Gamma_3 \neq 0$ (not to scale).**

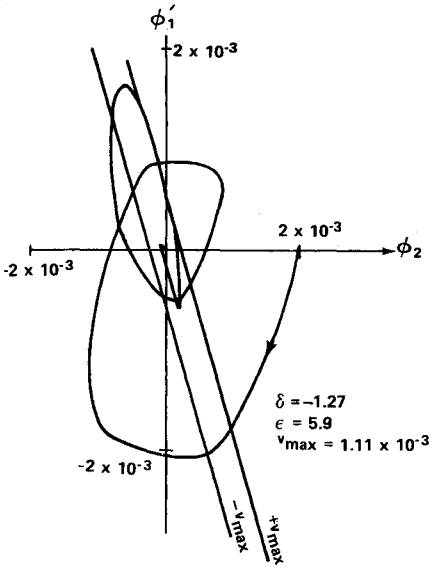


**Fig. 11** $\phi_2 - \phi_1'$ **control variable plane.**

switching conditions and the torque acting on the system [Eq. (9)] become

$$v_1 = v(\phi_2, \phi_1') \quad \text{if} \quad |v(\phi_2, \phi_1')| \leqslant v_{max}$$
$$v_1 = v_{max} \text{sign } v(\phi_2, \phi_1') \quad \text{if} \quad |v(\phi_2, \phi_1')| > v_{max} \tag{35}$$

where $v(\phi_2, \phi_1') = /\delta + \varepsilon)\phi_2 - \delta\phi_1'$. Hence, the wobble motion is prescribed by Eqs. (9) and (35), which characterize a piecewise linear motion. The character of the motion can be clarified on the $\phi_2 - \phi_1'$ control variable plane (Fig. 11). The two straight switching lines of Eq. (35) bound trajectories caused by linear control torques within the lines, and motion under the influence of constant saturation torque occurs when the trajectories lie outside the lines. A typical trajectory (Fig. 11) indicates that the choice of control parameters for the linear case still provides a response with bounds of the states that are comparable in magnitude to those resulting from the application of unlimited control torque.

## Conclusions

It has been shown that a simple model of a spinning rigid vehicle with two attached flexible booms can be actively controlled by the application of control torques. These torques are provided by onboard devices under the authority of a simple control postulate. Two control laws were considered: a simple attitude and attitude rate algorithm and an optimal control formulation. Using Skylab physical properties, stable operation and good dynamic responses are demonstrated. The effect of out-of-plane booms is investigated and shown to be inconsequential for Skylab. The effect of limited control torque is shown to affect the dynamic response, but limited analysis indicates that the effect is not deleterious. The results presented are now being compared with a more detailed 102 degrees-of-freedom spinning Skylab model implemented on a digital computer using a hybrid coordinate approach.[2,5] Initial results indicate good agreement between the analytical results of this paper and the digital computer results.

## References

[1] Seltzer, S. M., "Passive Stability of A Spinning Skylab," *Journal of Spacecraft and Rockets*, Vol. 9, No. 9, Sept. 1972, pp. 651–655.

[2] Seltzer, S. M., Justice, D. W., Patel, J. S., and Schweitzer, G., "Stabilizing A Spinning Skylab," *Proceedings of the 5th IFAC World Congress*, Paris, France, June 12, 1972.

[3] Chubb, W. B. and Seltzer, S. M., "Skylab Attitude and Pointing Control System," TN D-6068, Feb. 1971, NASA.

[4] Renard, M. L. and Rakowski, J. E., "Equatorial Vibrations of A Long Flexible Boom on A Spin Stabilized Satellite of Non-Zero Radius," *Proceedings of the 20th International Astronautical Congress*, Pergamon Press, New York, 1969, pp. 35–53.

[5] Likins, P. W., "Dynamics and Control of Flexible Space Vehicles," TR 32-1329, Rev. 1, Jan. 1970, NASA.

[6] Siljak, D. D., *Nonlinear Systems*, Wiley, New York, 1969.

[7] Bullock, T. E. and Fosha, C. E., "A General Purpose FORTRAN Program for Estimation, Control, and Simulation," *Proceedings of the Eighth Annual IEEE Region III Convention*, IEEE, New York, Nov. 1969, pp. 102–107.

[8] Bryson, A. E. and Ho, Y. C., *Applied Optimal Control*, Blaisdell, Waltham, Mass., 1969.

[9] Solheim, O. and Saelid, S., "Eigenvalue Sensitivity in Optimal Feedback Control Systems," 2nd IFAC Symposium on Multivariable Technical Control Systems, Oct. 1971, Duesseldorf, Germany.